Impact of Conifer Forest Litter on Microwave Emission at L-Band

Mehmet Kurum, *Member, IEEE*, Peggy E. O'Neill, *Senior Member, IEEE*, Roger H. Lang, *Fellow, IEEE*, Michael H. Cosh, Alicia T. Joseph, and Thomas J. Jackson, *Fellow, IEEE*

***Abstract*—This study reports on the utilization of microwave modeling, together with ground truth, and L-band (1.4-GHz) brightness temperatures to investigate the passive microwave characteristics of a conifer forest floor. The microwave data were acquired over a natural Virginia Pine forest in Maryland by a ground-based microwave active/passive instrument system in 2008/2009. Ground measurements of the tree biophysical parameters and forest floor characteristics were obtained during the field campaign. The test site consisted of medium-sized evergreen conifers with an average height of 12 m and average diameters at breast height of 12.6 cm. The site is a typical pine forest site in that there is a surface layer of loose debris/needles and an organic transition layer above the mineral soil. In an effort to characterize and model the impact of the surface litter layer, an experiment was conducted on a day with wet soil conditions, which involved removal of the surface litter layer from one half of the test site while keeping the other half undisturbed. The observations showed detectable decrease in emissivity for both polarizations after the surface litter layer was removed. A first-order radiative transfer model of the forest stands including the multilayer nature of the forest floor in conjunction with the ground truth data are used to compute forest emission. The model calculations reproduced the major features of the experimental data over the entire duration, which included the effects of surface litter and ground moisture content on overall emission. Both theory and experimental results confirm that the litter layer increases the observed canopy brightness temperature and obscure the soil emission.**

***Index Terms*—Forest, litter, microwave radiometry, radiative transfer, soil.**

I. Introduction

SOIL moisture (SM) is recognized as an important component of the water, energy, and carbon cycles at the interface between the Earth's surface and atmosphere, yet it is difficult to measure globally using traditional *in situ* techniques. Several planned L-band space missions, including the European Space Agency Soil Moisture and Ocean Salinity (SMOS) and NASA's Soil Moisture Active Passive (SMAP) (to be launched in 2014) satellites, are focusing on obtaining accurate SM information over as much of the Earth's land surface as possible [1], [2]. One of the ongoing challenges is to extend the retrievals to forested areas, which constitutes approximately 30% of the Earth's land surface. The contributions of both the canopy and the underlying surface to the measured brightness temperature need to be understood if we expect to retrieve SM. In order to fully exploit microwave radiometric data in SM retrievals over vegetated landscapes, measurements using airborne and ground-based radiometers at L-band have been made [3]–[11]. In addition, several theoretical emission models have been developed and successfully validated in many cases [12]–[19].

Over the past few years, some attention has been placed on understanding the microwave signatures of deciduous and coniferous forest floors [8]–[10], [16], [17]. Several field experiments have demonstrated the significance of a forest litter layer in SM retrieval from L-band brightness data [5], [8], [20]. It has been hypostatized that litter layer increases the forest floor emissivity, particularly when wet, as compared with soil. The modeling of conifer needle litter at L-band using a microwave radiative transfer (RT) model [12] in conjunction with ground truth measurements has been demonstrated by Della Vecchia *et al.* [16]. Schwank *et al.* [17] developed a physically based model of the microwave radiation of leaf litter for different moisture conditions. Both of these modeling efforts [16], [17] confirmed the aforementioned experimental observations and concluded that when the litter is wet, it acts as an important source of radiation. Laboratory observations of the dielectric properties of litter were made by Kleshchenko *et al.* [21] and Demontoux *et al.* [22]. Grant *et al.* [10] made *in situ* field observations of forest floor layers in their undisturbed state by sequentially stripping each layer. This was the first investigation to use *in situ* experimental data in this context. Their results provided some insight into the relative contribution of each forest floor layer to the overall zero-order emission at L-band.

Although some progress has been made in understanding the contribution of forest litter to the overall emission, the number of *in situ* field observations of forest floor layers is still sparse and includes only a limited set of forest covers and radiometric configurations. More efforts are required to solidify our scientific understanding of forest floor effects on microwave spaceborne radiometric observations over different types of vegetated landscapes in order to optimally utilize spaceborne radiometric data in global SM retrievals. This study provides a

Manuscript received November 15, 2010; revised June 21, 2011; accepted July 31, 2011. This work was supported by an appointment to the NASA Postdoctoral Program at the Goddard Space Flight Center administered by Oak Ridge Associated Universities through a contract with NASA.

M. Kurum, P. E. O'Neill, and A. T. Joseph are with the Hydrological Sciences Branch, Code 614.3, NASA Goddard Space Flight Center, Greenbelt, MD 20771 USA (e-mail: mehmet.kurum@nasa.gov; peggy.e.oneill@nasa.gov; Alicia.T.Joseph@nasa.gov).

R. H. Lang is with the Department of Electrical and Computer Engineering, George Washington University, Washington, DC 20052 USA (e-mail: lang@gwu.edu).

M. H. Cosh and T. J. Jackson are with the Hydrology and Remote Sensing Laboratory, Agricultural Research Service, U.S. Department of Agriculture, Beltsville, MD 20705 USA (e-mail: Michael.Cosh@ars.usda.gov; tom.jackson@ars.usda.gov).

Color versions of one or more of the figures in this paper are available online at http://ieeexplore.ieee.org.

Digital Object Identifier 10.1109/TGRS.2011.2166272

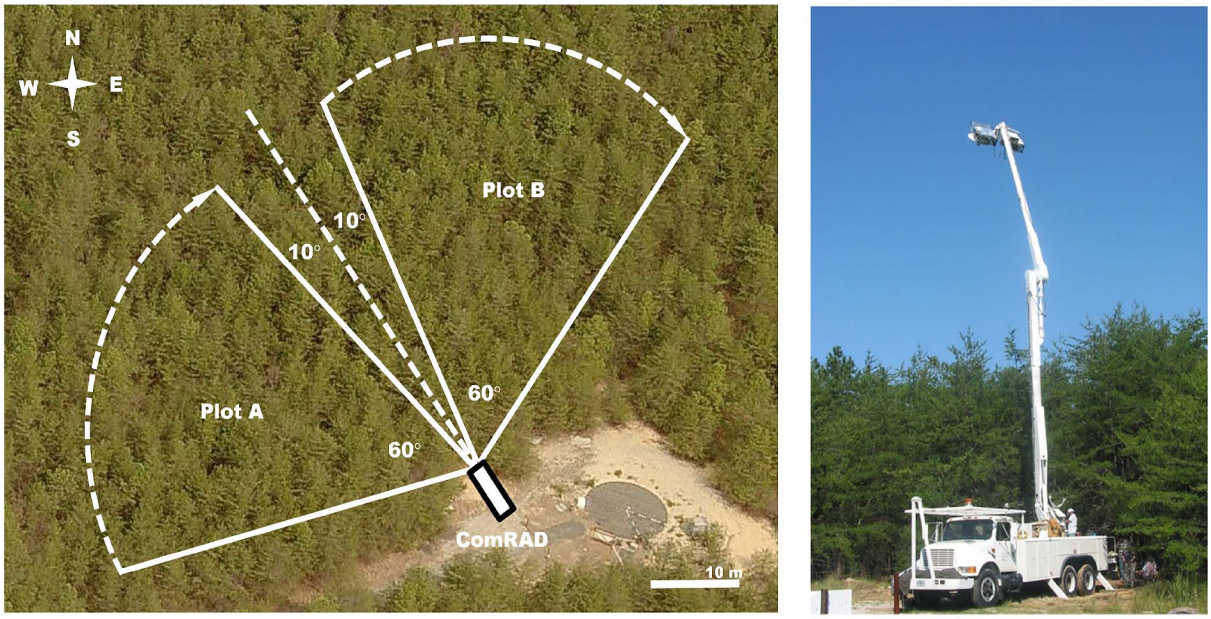

Fig. 1. (a) Natural Virginia pine forest site at Goddard Geophysical and Astronomical Observatory. (b) ComRAD microwave instrument system deployed over a natural stand of Virginia pine forest.

new *in situ* experimental data set acquired for a pine forest site and adapts a previously developed first-order RT model [19] to conifer trees, which includes a new representation of the forest floor as a surface layer of loose debris/needles and an organic transition layer above the mineral soil.

In the study by Grant *et al.* [10], observations of the forest floor were made with ground-based instruments located below the canopy. Microwave measurements in this investigation were acquired from above the conifer canopy. Multiangular observations were obtained at horizontal and vertical polarizations on ten different days over a year to include temporal information on ground properties. In addition, on a day with wet soil conditions, an experiment was conducted in which the surface litter layer was removed from one half of the test site within a short period of time while keeping the other half undisturbed. The experiment was intended to study the impact of surface litter layer on microwave emission from forested terrain at L-band.

One of the most distinctive features of the data set that will be presented is the observation of considerable change in brightness temperature after the litter was removed. The other important aspect of the data set is the limited radiometric sensitivity to the underlying ground moisture through the pine tree canopy even though the volumetric moisture content (VMC) of the ground varied from 0.05 to 0.30 $\mathrm{cm}^3 \cdot \mathrm{cm}^{-3}$. These observations were investigated by using a first-order RT model of forest canopy [19] with an underlying multilayer forest floor. The model predictions were in good agreement with the data, with limited discrepancies, and provide a quantitative understanding of the influence of organic layers on the first-order brightness temperature. The model results show that the addition of organic layers on top of the mineral soils produces an increase in the overall emission and the first-order scattering contribution, which is also found to be fairly constant over the wide range of ground moisture. The lack of ground moisture sensitivity was attributed to the presence of the surface litter layer which masks soil emission. The effect of surface litter is found to be more evident when the litter is wet and negligible under dry conditions. This study not only confirms the aforementioned recent modeling and experimental observations but also, to our knowledge, is the first to use a first-order RT model in conjunction with *in situ* experimental data in forest litter investigations.

The description of the experimental site and the procedure for data collection are discussed in Section II, where the ground truth and canopy geometry parameters needed for the model are also given. Formulations of a microwave radiometry model of the canopy and the multilayer forest floor are briefly described in Section III. The interpretation of radiometer data by using model and other ground information is discussed in Section IV.

II. Experiment Site and Data Collection

In 2008–2009, field experiments involving ComRAD (Combined Radar/Radiometer), an L-band active/passive truck system [23], were conducted over a natural stand of Virginia Pine (*Pinus virginiana*) trees located near the NASA Goddard Space Flight Center, Maryland (latitude 39° 1′ 21.18″ N, longitude 76° 49′ 28.02″ W, altitude 55 m). The site was divided into two equal plots of 60° azimuth sectors with similar tree and ground characteristics. Fig. 1(a) shows an aerial view of the test site with an illustration of the plot sectors. Fig. 1(b) shows a picture of the ComRAD microwave instrument system deployed over the forest site.

The site under investigation is a Virginia Pine forest stand with an average height of 12 m and basal area of 34 $\mathrm{m}^2 \cdot \mathrm{ha}^{-1}$.

TABLE I
EXPERIMENT SITE INFORMATION

LOCATION:	NASA GSFC's Goddard Geophysical and Astronomical Observatory (GGAO) campus in Greenbelt, Maryland, USA
FOREST TYPE	Natural Virginia Pine Trees (*Pinus virginiana*)
TREE HEIGHT:	12 m
DIAMETERS AT BREAST HEIGHT:	Varying 2 – 34 cm with an average of 12.6 cm
BASAL AREA:	34.0 m^2 ha^{-1}
WOODY VOLUME:	310.9 m^3 ha^{-1}
BULK DENSITIES:	1.11 $g.cm^{-3}$ (mineral soil), 0.15 $g.cm^{-3}$ (organic humus layer), 0.10 $g.cm^{-3}$ (surface litter layer)
MINERAL SOIL :	Loamy Sand - varying from 57 % sand, 14 % clay to 87 % sand, 3 % clay depending on location within the site.
SURFACE ROUGHNESS :	RMS roughness height < 0.5 cm
TP READINGS RANGE :	0.05 – 0.30 cm^3 cm^{-3}

Virginia Pine is a medium-sized evergreen conifer that is native to North America. The bark is thin and dark reddish-brown and is broken into shallow plates. The short needles (4–8 cm) of Virginia Pine range from dark green to gray green to yellow green and are usually twisted and in pairs. These trees have a tendency to maintain a substructure of needleless dead branches. The forest under investigation is very homogenous, with a distinct needle litter layer over an organic humus transition layer with an underlying well-drained mineral soil. The results of detailed measurements characterizing the trees and forest floor will be given in Sections II-C and II-D. A summary of site characteristics are given in Table I.

A. Instrumentation

ComRAD is mounted on a 19-m hydraulic boom truck [Fig. 1(b)]. The system includes a dual-pol 1.4-GHz radiometer and a quad-pol 1.25-GHz radar sharing the same 1.22-m parabolic dish antenna with 3-dB beamwidth of approximately 12°. ComRAD's radiometer is a total power radiometer with a two-point internal calibration. The absolute accuracy and the sensitivity of the instrument are ± 1 K and ± 0.1 K, respectively. For internal calibration, the cold source is implemented by an amplifier terminated by a 50-Ω matched microwave load with an isolator attached to the input and the hot source is made up of a commercial hot noise source along with an attenuator. The radiometer has an internal physical temperature of 45 °C, reference hot sources of 401.2 K and 395.4 K for horizontally and vertically polarized signals, respectively, and cold sources of 154.5 K and 142.7 K for horizontally and vertically polarized signals, respectively. The noise characteristics of the internal calibration sources are determined as a function of internal ambient temperature at the beginning of each field campaign. External calibration of the radiometer is carried out during each measurement run to correct for temperature variation and loss in the cables connecting the receiver to the antenna and for variation in the antenna temperature. This external calibration is achieved using cold sky and ambient microwave absorber targets.

B. Microwave Measurements

The experiment site consists of two equal plots of 60° azimuth sectors with similar tree and ground characteristics. Microwave active/passive data were obtained on August 1, 4, 20, and 30, September 8, and November 20 in 2008, and on April 8 and 23 and August 4 and 18 in 2009. The experiment conducted on April 23, 2009 involved the removal of the surface litter layer from one half of the test site while keeping the other half undisturbed (see Section IV). In this paper, an analysis of only the radiometer observations is presented. Radiometer data were acquired at a height of 19 m above the ground level with incidence angles of 15°, 25°, 35°, 45°, and 55°. The areas of the corresponding footprints on the ground at these angles were 16.5, 20.1, 27.4, 43.1, and 83.0 m^2, respectively. Data were usually collected over a time span of about 2 h during early morning. During the radiometer measurements, the truck boom was rotated in azimuth at 15° increments within a 60° azimuth span in each plot. The resulting radiometer data for the tree plot at each incidence angle is an average of data from the three azimuthal observation locations. The total precipitation and average temperature for the entire duration of the campaign were 1080.5 mm and 13.1 °C at a metrological station located less than 2 km away. No precipitation occurred during any of the microwave measurements.

C. Ground Sampling

The site under investigation is a typical pine forest site with a forest floor made up of organic matter generated by the canopy. This material can be characterized by litter and humus layers lying on the mineral soil surface. There are distinct boundaries between each of the layers, as shown in Fig. 2(a). The top litter layer is composed of loose debris/needles that have undergone little or no decomposition. Next is a humus layer, which is a transition layer of partially and fully decomposed organic materials lying immediately above the mineral soil. The composition of the mineral soil is loamy sand, with textures varying from 57% sand, 13.6% clay to 87% sand, 3.4% clay depending on its location within the site. A geometric illustration of the forest floor system over the site is given in Fig. 2(b).

Coincident with the microwave measurements, ambient canopy temperatures were obtained at approximately the same look angle as the microwave instruments using an Apogee[1] thermal infrared radiometer (8–14 μm) mounted on the ComRAD instrument platform. After the microwave measurements were completed at each incidence angle, Dynamax ML2x[1] Theta Probes (TPs) and handheld infrared thermometers were used to obtain VMC and surface soil temperature, respectively.

[1]This product is for informational purposes only, and its citation here should not be considered an endorsement of the product.

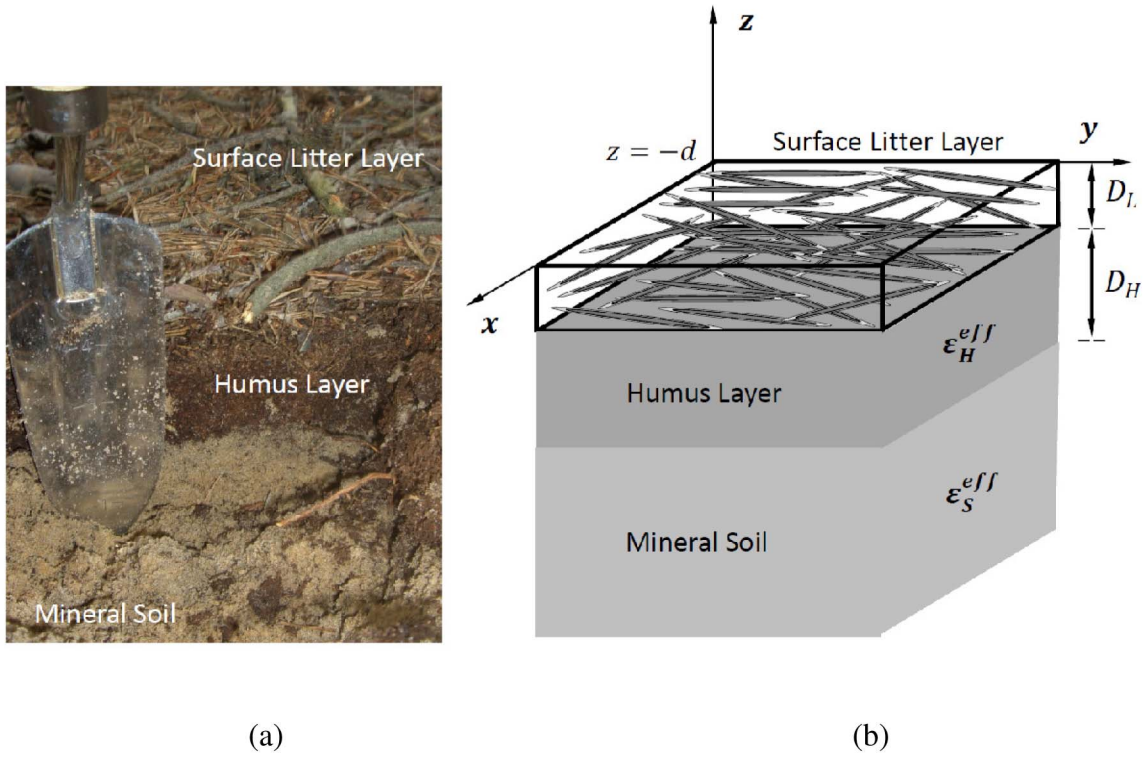

Fig. 2. (a) Photograph from the pine forest floor. (b) Illustration of the pine forest floor.

TABLE II
AVERAGE AMBIENT TEMPERATURES AND TP READINGS

`PLOT AVERAGES	AMBIENT TEMPERATURE [°C]		TP READINGS [$cm^3.cm^{-3}$]	
MEASUREMENT DATES	PLOT A	PLOT B	PLOT A	PLOT B
1-AUG-08	29.1	30.1	0.12	0.10
04-AUG-08	24.1	24.4	0.11	0.09
20-AUG-08	21.4	21.4	0.07	0.05
30-AUG-08	21.8	21.9	0.14	0.11
8-SEP-08	23.3	23.1	0.15	0.15
20-NOV-08	3.2	3.7	0.17	0.15
8-APR-09	4.8	5.7	0.24	0.20
23-APR-09	9.6	10.2	0.27	0.21
23-APR-09*	12.5	13.8	0.25	0.20
04-AUG-09	26.7	26.5	0.14	0.13
18-AUG-09	26.1	27.0	0.06	0.04
*Ground measurements after litter removal				

Ground measurements were taken at four arbitrary locations within each field of view (generally 20 samples in each plot) and subsequently averaged for each incidence angle. Average ambient temperatures and *TP* readings are provided in Table II. A wide range of ground moisture (TP readings varied from 0.05 to 0.30 $cm^3 \cdot cm^{-3}$) under the pine trees was encountered during the entire campaign.

TABLE III
AVERAGE LAYER THICKNESSES

	LITTER(L)	HUMUS (H)
THICKNESS	[cm]	[cm]
MEAN	$D_L = 0.8$	$D_H = 2.2$
STANDARD DEV.	$\delta D_L = 0.3$	$\delta D_H = 0.9$

The TP instruments were inserted vertically into the first 6-cm depth of the forest floor. The average thickness of the litter layer was 0.8 cm while the same parameter for humus layer was 2.2 cm (see Table III). Since the TP readings provided combined VMCs of the three layers, specific measurements of gravimetric moisture content (GMC) in $kg \cdot kg^{-1}$ and bulk density need to be carried out for each layer in order to separate the volumetric moisture contributions of the single layers. In addition to the regular ground measurements as described above, separate direct measurements of GMC, bulk density, and thickness of litter and humus layers coincident with dielectric TP measurements were made at 20 arbitrary locations within the radiometer footprints on four days (see Table IV). The average TP readings on these days varied from 0.06 to 0.25 $cm^3 \cdot cm^{-3}$, which is similar to the range of measurements encountered over the entire campaign. The GMC data from the destructive sampling of the litter and humus layers allowed us to conduct gravimetric calibration of entire TP data for the layer depths, which resulted in the following empirical relationships:

Litter Layer

$$GMC = 6.3294 \times TP - 0.0187, \quad R^2 = 0.9296 \qquad (1a)$$

TABLE IV
GRAVIMETRIC CALIBRATION OF EACH LAYER. TP AND GMC VALUES ARE MEASURED. VMC VALUES FOR BOTH LAYERS ARE CALCULATED USING (1d)

PLOT B AVERAGES	THETA PROBE (TP)	LITTER LAYER		HUMUS LAYER	
MEASUREMENT DATES	READINGS [$cm^3.cm^{-3}$]	GMC [kg .kg^{-1}]	VMC [$cm^3.cm^{-3}$]	GMC [kg .kg^{-1}]	VMC [$cm^3.cm^{-3}$]
23-APR-09	0.25	1.53	0.15	2.08	0.31
04-AUG-09	0.10	0.83	0.08	0.68	0.10
18-AUG-09	0.06	0.21	0.02	0.27	0.04
15-SEP-09	0.14	0.84	0.08	0.86	0.13

Humus Layer

$$GMC = 9.371 \times TP - 0.3153, \quad R^2 = 0.9791 \qquad (1b)$$

where GMC denotes gravimetric moisture content, which is defined on dry basis by

$$GMC = W_W / W_D \qquad (1c)$$

with the water weight W_W and the weight of the dry matter W_D in kilograms. The GMC is also related to VMC by

$$VMC = \rho_b \times GMC \qquad (1d)$$

where the quantity ρ_b is the bulk density. The measured bulk densities for the litter, humus, and mineral soil layers are 0.10, 0.15, and 1.11 g $\cdot$ cm^{-3}, respectively.

In addition to the gravimetric calibration of each layer, the surface roughness properties of the forest floor were estimated by inserting a gridded metal sheet into the floor vertically and photographing it. The photo was corrected for viewing angle variation, and the surface was digitized. From this digital surface, the surface rms height was calculated as less than 0.5 cm.

D. Tree Sampling

Ground measurements of trees were carried out in 2009. The collection of tree data involved the measurement of tree diameter and height, branch dimensions and orientations, needle statistics, and the dielectric constants of each tree constitution type. The forest is estimated to be 12 m high, and there are total of 332 trees within the footprints of all look angles (15°–55°) in both plots. The average tree density is calculated to be 0.02075 trees per m^2, and the basal area was 34 $m^2 \cdot ha^{-1}$. A series of Leaf Area Index (LAI) measurements were made with an LAI-2000 (LiCor[1]) on September 17, 2009. The average LAI was 2.66 with a standard deviation of 0.16, which indicates a very homogeneous vegetation canopy.

The diameters at breast height (DBHs) of all the trees within the footprints were measured. The measured DBH distribution is shown in Fig. 3. The DBH of all measured trees varied from 2 to 34 cm with a mean DBH of 12.6 cm and a standard deviation of 7 cm. The tree DBH data were redistributed into two categories based on their sizes, each representing a typical tree in the site. Seventy percent (70%) of the measured trees had DBH values less than 17 cm, and their average DBH was 9.2 cm with a standard deviation of 4 cm. The mean DBH of the rest of the trees was 22.5 cm with a standard deviation of 3.4 cm. For determination of the tree architecture, two representative Virginia Pine trees having DBH values equal to 9 and 23 cm and a height of about 12 m were chosen for canopy geometry measurements. The detailed size and orientation statistics of needles, branches, and trunks were acquired by cutting down the trees. The results from the canopy sampling are shown in Table V.

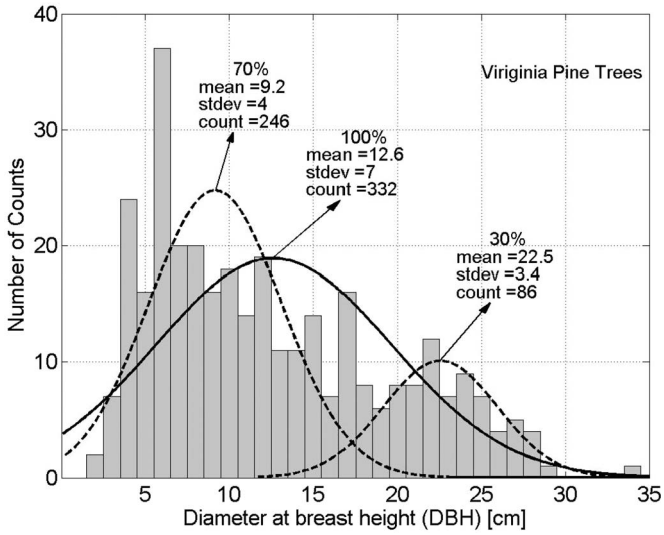

Fig. 3. Measured DBH within the footprint. The solid line shows the normal DBH distribution of all trees in both plots while dashed curves represent normal DBH distribution of two categories of typical trees with average DBHs of 9.2 and 22.5 cm.

The diameter profile of the trunks was also measured by sampling at successive intervals of height. The average height trunk was divided into equal length cylinders, and an average diameter was determined for each interval. The volumes of the equivalent tapered trunk for the trees having DBH values equal to 9 and 23 cm were 0.0429 and 0.2933 m^3, respectively, which were then used to calculate equivalent trunks having a constant diameter (same volume but different dimensions). An equivalent cylinder model based only on constant volume is assumed.

The trees at the study site had a substructure of needleless branches (dead). Live as well as dead branches are further

TABLE V
CANOPY PARAMETERS FROM DESTRUCTIVE SAMPLING

TREE COMPONENTS	PARAMETERS				
	AVERAGE LENGTH [cm]	AVERAGE RADIUS [cm]	DENSITY [m^{-3}]	DIELECTRIC	ORIENTATION
TRUNKS	706	11.50	0.0051	14.5+i2.9	*Vertical*
	674	4.50	0.0117	14.5+i2.9	*Vertical*
NEEDLES	6	0.05	5414	18.4+i3.3	*Uniform [0º – 90º]*
BRANCHES (LIVE)	285	1.31	0.2519	10.8+i2.6	*Uniform [60º – 90º]*
	69	0.38	3.7	13.3+i2.8	*Uniform [0º – 90º]*
	26	0.18	22.7	13.3+i2.8	*Uniform [0º – 90º]*
BRANCHES (DEAD)	50	0.54	0.4428	5.0+i1.0	*Uniform [70º – 90º]*
	140	1.25	0.1416	5.0+i1.0	*Uniform [70º – 90º]*

grouped based on diameter sizes. An average length and an average diameter were determined for each of the classes of branches. The total number of branches in each branch class was recorded. The density of each branch class was found by determining the total number of branches of that type in the forest plot and then dividing by the total volume of the forest (average height times plot area). The number of scatterers of each type in the plot was determined from the counts made on the sampled tree times the number of the trees in the plot.

The needle dimensions and needle density per unit length on a shoot was measured. From a knowledge of the number of shoots and subshoot on an individual tree, an estimate of the number of needles per tree can be obtained. Calculations based on the sampled trees with DBH values equal to 9 and 23 cm resulted in approximately 111 000 and 950 000 needles, respectively. The average density of needles per unit volume is computed to be 5414 needles per m^3. Even though there are several different types of needles, all needles were put into one class for modeling purposes. This is because the contribution of needles at L-band to the total backscattering response is expected to be negligible as compared with the contribution from branches and trunks. Needles contribute mostly to the canopy extinction properties. As a result, using one class for needles was found satisfactory. The needles are modeled as a thin dielectric cylinder with length of 6 cm and equivalent diameter of 0.5 mm. The angular distribution of the needles is taken to be uniform.

The relative dielectric constants of the tree constituents were measured at L-band (1.25-GHz) *in situ* using dielectric probes connected to an HP8719A vector network analyzer. The technique is based on reflection from an open-ended coaxial probe. The measured average relative dielectric constants are $18.4 + \mathrm{i}3.3$ for needles, $10.8 + \mathrm{i}2.6$ for primary live branches, $13.3 + \mathrm{i}2.8$ for secondary live branches, $5.0 + \mathrm{i}1.0$ for dead branches, and $14.5 + \mathrm{i}2.9$ for trunks.

III. MICROWAVE MODELING

A first-order microwave model based on an iterative solution of RT equations has been recently developed and successfully validated with data collected over deciduous trees [19]. In this section, the microwave model is adapted to coniferous trees with an underlying multilayer forest floor.

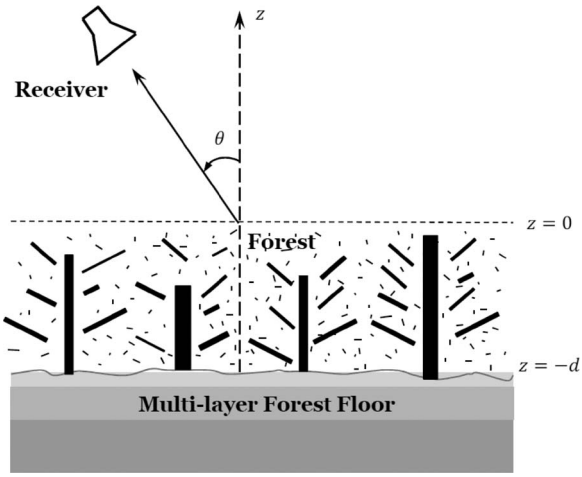

Fig. 4. Schematic diagram of a pine forest.

Fig. 4 shows an illustration of the forest model that will be employed here. The forest canopy of thickness d is modeled as a slab containing a random distribution of dielectric cylinders. The cylinders are circular, homogenous, and lossy, and their dimensions and orientations are typical of trunks, branches, and needles. It is assumed that cylinders are distributed uniformly in the azimuthal coordinate. The slab of cylinders is placed over a three-layer lossy dielectric half space representing the forest floor. The forest floor is modeled as a three-layer soil that includes a litter layer (loose debris/needles), a transition layer (organic humus), and mineral soil. The interface between the ground and canopy is assumed to be rough.

A. First-Order RT Model ($\tau-\omega-\Omega$ Model)

The first-order model is based on an iterative solution of the RT equations by interpreting the scattering source function as a perturbation to the nonscattering RT equations [19]. This formulation adds a new scattering term to the $\tau-\omega$ (tau–omega) model that is an easily implemented and theoretically simple zero-order RT approach. The improved model has the

advantage over the conventional tau–omega model because the first-order solution accounts for scattering of the radiated emission from ground and the vegetation layer. The first-order solution from the forest canopy leads to an expression given by

$$e_p^{(1)}(\theta) = \left[1 - \gamma_p^2(\theta) R_p^{\mathrm{FF}}(\theta)\right] - \omega_p(\theta)\left[1 + \gamma_p(\theta) R_p^{\mathrm{FF}}(\theta)\right] \times \left[1 - \gamma_p(\theta)\right] + \Omega_p(\theta) \quad (2a)$$

where the ambient temperatures of the vegetation layer and the ground are assumed to be same, $R_p^{\mathrm{FF}}(\theta)$ is the microwave reflectivity of the forest floor that will be described in next section (Section III-B), $\gamma_p(\theta)$ is the vegetation transmissivity which is parameterized as $\gamma_p(\theta) = \exp(-\tau_p(\theta)\sec\theta)$ where $\tau_p(\theta)$ is the vegetation opacity or optical thickness and θ is the incidence angle, and $\omega_p(\theta)$ is the single scattering albedo. The polarization p can be horizontal (h) or vertical (v). The last term $\Omega_p(\theta)$ will be described next.

The first term in (2a) represents the nonscattering case (independent of scattering albedo) and is also equivalent to the zero-order solution of the albedo expansion for canopies having uniform physical temperature profiles [13]. The second term represents scattering darkening due to albedo. The combination of the first two terms represents the zero-order solution (tau–omega model). The parameter $\Omega_p(\theta)$ denotes the additional scattering contribution to the zero-order model. It represents the emission from the ground and the vegetation layer that is single-scattered from tree trunks, branches, and needles. The scattering component $\Omega_p(\theta)$ is composed of eight terms representing different scattering mechanisms which are given by

$$\Omega_p(\theta) = \sum_j \left\{\Omega_{jp}^{(s1)}(\theta) + \Omega_{jp}^{(sr1)}(\theta)\right\}, j \in \{G, U, D, DG\} \quad (2b)$$

where the summation index j denotes the scattering-mechanism types, i.e., the subscripts G, U, D, and DG refer to the scattered radiation contributions due to ground emission, upwelling emission, downwelling emission, and downwelling emission followed by ground reflection, respectively. The scattered radiation from each mechanism arrives at the receiver either directly (denoted by $s1$) or through reflection from the ground (denoted by $sr1$). A pictorial illustration of the scattering processes and the explicit expressions for each scattering term are given in Kurum *et al.* [19].

B. Three-Layer Forest Floor Model

The basis of TP measurements is the apparent dielectric constant of the soil, which changes with moisture content. Empirical and dielectric mixing models [25]–[31] are used to relate VMC to effective dielectric properties of various soil types. Due to the differences in bulk density and surface area of materials constituting each forest layer, this relationship in organic soils is very different than the relationship found in mineral soils [29], [30]. Each forest floor layer (surface litter, humus, and mineral soil) must be treated separately [32]. As seen in Fig. 2(a), the forest floor under investigation is made up of distinct layers with easily observable boundaries and could be modeled as three dielectric slabs [see Fig. 2(b)]. An anisotropic effective medium approach with a three-phase dielectric mixing model [33] is applied to represent the highly complex nature of the surface litter layer. The effective dielectric properties of organic humus [31] and mineral [28] soil layers are obtained from empirical relations published in the literature.

1) *Mineral Soils*: Empirical and dielectric mixing models have been developed in the past to relate water content to bulk dielectric permittivity of mineral soils [24]–[28]. In this paper, the Dobson model [28] is used to estimate the dielectric constant $\varepsilon_S^{\mathrm{eff}}$ of the mineral soil layer.
2) *Organic Soils*: The models developed for mineral soils cannot be applied to organic soils due to the presence of high porosity combined with the large amounts of "bound" water found in organic soils [30]. Schaap *et al.* [31] developed an empirical model for organic humus layer that accounts for the bulk density of the humus organic soil. This model was calibrated by using 25 forest samples of five different forest stands, all of which were situated on sandy soils and had a sharp boundary with the mineral horizon, similar to forest floor conditions under investigation here. In this paper, the Schaap empirical model is used to estimate the dielectric constant $\varepsilon_H^{\mathrm{eff}}$ of the organic humus layer. The real part of the dielectric constant is given by

$$\varepsilon_{Hr}^{\mathrm{eff}} = \left(\left[(VMC)^{1/0.885(\pm 0.018)} + 0.146(\pm 0.002)\right] / \left[0.133(\pm 0.002)\right]\right)^2 \quad (3)$$

where the VMC of the humus layer is obtained from TP readings using the relationship given in (1b). The imaginary part of the dielectric constant $\varepsilon_{Hi}^{\mathrm{eff}}$ is specified to be one tenth of the real part [34].
3) *Litter Model*: A three-phase dielectric mixing model [33] is applied for estimating the effective dielectric properties of the surface litter layer as described in the Appendix. The mixing scheme consists of inclusions made up of an organic core and outer water shell of confocal prolate ellipsoids in the background of free space. The inclusions are situated in all directions parallel to the soil–surface plane. This arrangement accounts for the general shape and axial alignment of the fallen needles in the litter via the depolarization factor as well as phase configuration effects. Different litter moisture states are considered by means of shells with a different thickness of water coating each ellipsoid. The total volume of these shells with bound water is used to represent the water volume retained in the litter per volume.

The real part of dielectric constant of the ground layers has the most influences on the overall reflectivity. Fig. 5 shows plots of the real part of effective dielectric constants for mineral soil, humus, and litter layers as a function of TP readings. To generate the graph, TP measurements are converted to the VMCs of

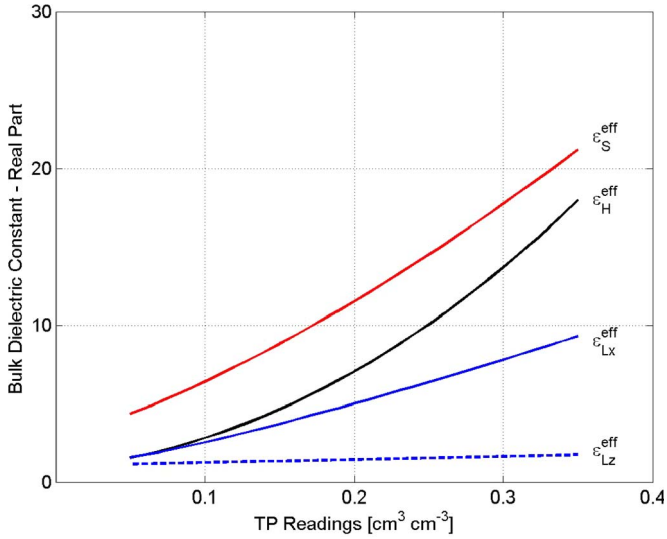

Fig. 5. Effective dielectric constants of soil ($\varepsilon_S^{\text{eff}}$), humus ($\varepsilon_H^{\text{eff}}$), and litter ($\varepsilon_{Lx}^{\text{eff}}$ in horizontal direction and $\varepsilon_{Lz}^{\text{eff}}$ in vertical direction) layers.

each layer using the site-specific calibration coefficients given in (1). These VMCs are the input variables required to compute the permittivities using the Dobson model for the mineral soil, (3) for the humus, and the mixing model presented in the Appendix for litter. Due to the high porosity and large amounts of "bound" water found in organic layers, their dielectric constants are lower than the dielectric constant of mineral soil, which can be seen in the plots. Since the surface litter is more porous than the humus layer, their dielectric constant is the lowest of the three layers. This incremental change in dielectric constants in the forest floor layers behaves similar to matching layers that reduce the dielectric discontinuity between air and deeper soil layers [16], [17].

A coherent model representing the three-layer forest floor (litter–humus–mineral soil) as a stratified dielectric medium is used to compute the coherent floor reflectivity $R_p^{\text{coh}}(\theta)$. The model is based on a matrix formulation of the boundary conditions at dielectric discontinuities derived from Maxwell's equations [35]. The anisotropic nature of the litter layer (loose debris/needles) in the spatial domain was included in the coherent reflectivity calculations to keep the morphology as close as possible to reality. There are no approximations involved in the calculation of the coherent reflectivities except the aforementioned use of estimated permittivities. The results are direct consequences of Maxwell's equations. Even though there is a significant difference between the calculated litter permittivities in vertical and horizontal directions ($\varepsilon_{Lz}^{\text{eff}}$ and $\varepsilon_{Lx}^{\text{eff}}$), as indicated in Fig. 5, the effect of litter spatial anisotropy on the overall forest emission was found to be negligible compared with the simulation using an isotropic litter layer model, where the inclusions are oriented randomly. This is mainly because the contribution of the vegetation (forest canopy) layer dominates the overall emission and masks the anisotropic nature of the litter layer whose thickness is very thin.

The coherent forest floor reflectivity exhibits oscillations due to alternating constructive and destructive interferences between waves reflected at the surface. However, this coherent effect is smoothed by the natural variations of the layer thicknesses around its average value. Therefore, the coherent reflectivities are averaged over the thickness range of the layers in order to represent the natural variation of larger thicknesses throughout the forest. This average reflectivity is given by

$$R_p^{\text{avg}}(\theta) \cong \int_{D_H-2\delta D_H}^{D_H+2\delta D_H} \int_{D_L-2\delta D_L}^{D_L+2\delta D_L} R_p^{\text{coh}}(\theta).p(D_L, D_H)dD_L dD_H \tag{4}$$

where $p(\cdot)$ is Gaussian probability density. The humus and litter later thicknesses are denoted by D_L and D_H, respectively. Average layer thicknesses and their variations are given in Table III.

The average reflectivity $R_p^{\text{avg}}(\theta)$ is then corrected by modifying it with the well-established Kirchhoff's approximation with a small height standard deviation [36]. For the study field, the surface rms height was on the order of 0–0.5 cm, which is rather low compared with the L-band wavelength. As a result, only the coherent component of the roughness is important for this study and the diffuse component is ignored. The reflectivity of the effective rough surface is expressed as

$$R_p^{\text{FF}}(\theta) = R_p^{\text{avg}}(\theta)e^{-h\cos^2\theta} \tag{5}$$

where the roughness height parameter is given by $h = 4\sigma^2 k_0^2$ in terms of the surface rms height σ and the wavenumber $k_0 = 2\pi/\lambda_0$, where λ_0 is the free-space wavelength. The resulting reflectivity $R_p^{\text{FF}}(\theta)$ is used to describe reflectivity of the forest floor given in (2a) of the first-order RT model.

IV. Results and Discussion

An experiment was conducted on April 23, 2009, when the ground was wet, with the intention of characterizing and modeling the impact of the surface litter layer on the observed emissivity. The experiment consisted of removing the surface litter layer from one half of the test site while keeping the other half undisturbed. On the day of the experiment, a set of baseline microwave measurements and ground truth data were obtained over two adjacent plots (A and B) in early morning. Right after the baseline measurements, the litter layer was removed from Plot A (about 700-m^2 area) in less than 2 h. Following the removal, the measurements were repeated for both plots. Images of the litter layer and of the pine tree site after the litter removal are shown in Fig. 6.

In Fig. 7, the measured microwave emissivities (the ratio of the measured brightness and the ambient temperatures) for both plots on April 23 are graphed as a function of the incidence angle. The filled markers represent data collected before the litter removal, and the nonfilled markers represent data collected after the litter removal. During the 2-h period of litter removal, the physical scene temperature increased by about 2 °C, and the TP readings decreased by about 0.02 cm$^3 \cdot$ cm^{-3}, as shown in Table VI. Fig. 7(b) shows that there was almost no change in emissivity for Plot B, which demonstrated in the stability of the radiometer calibration during the data collections. On the other hand, the data show a detectable decrease (particularly at

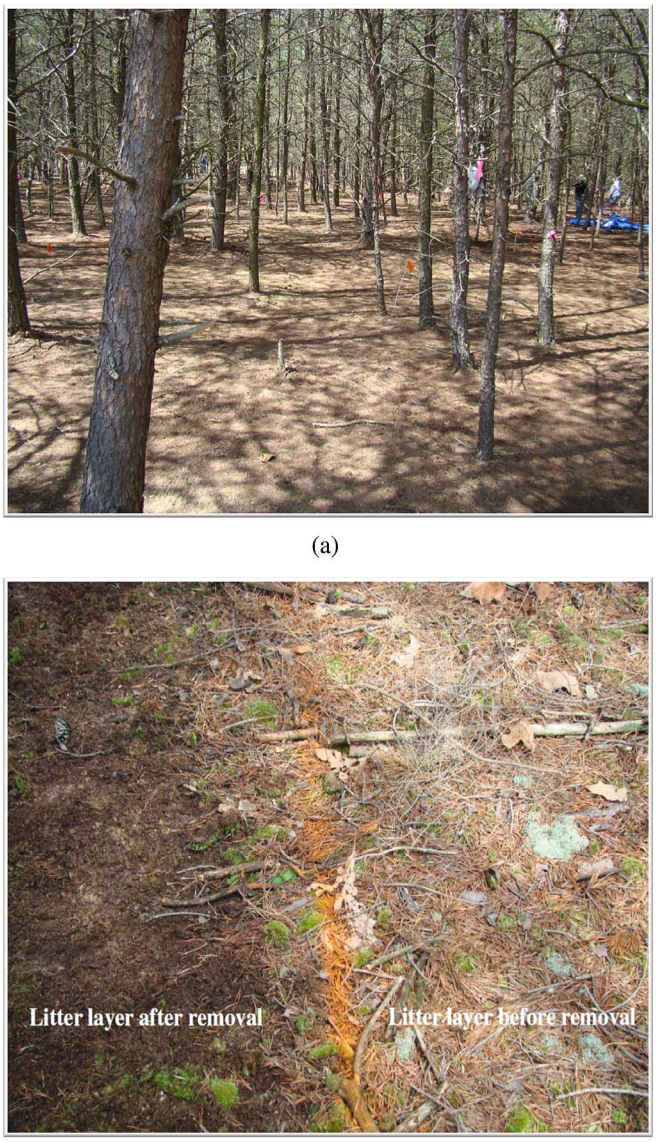

(a)

(b)

Fig. 6. (a) Plot A after removal of surface litter layer. (b) Forest floor with/without litter removal.

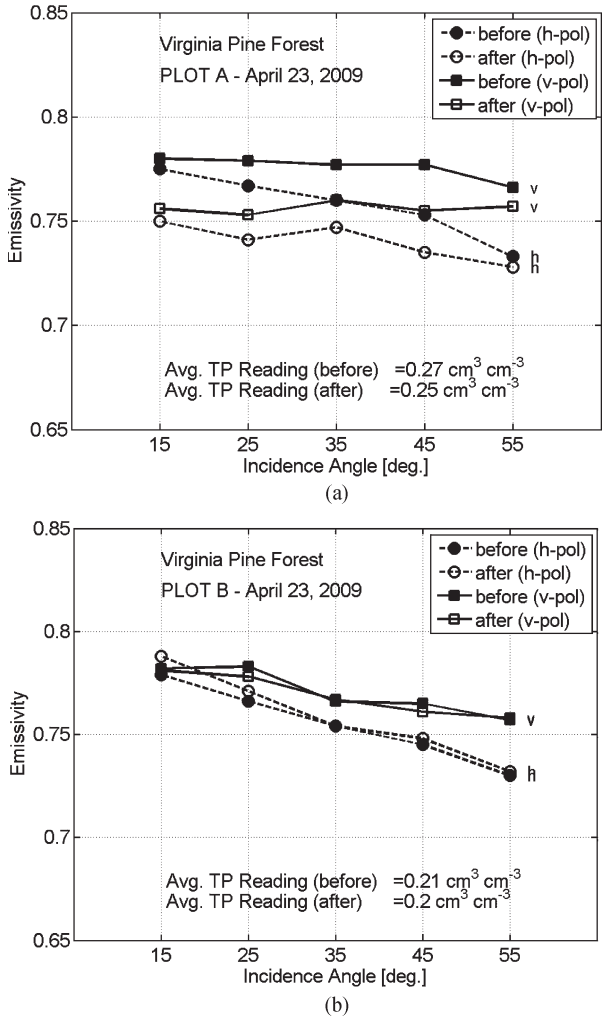

(a)

(b)

Fig. 7. Measured L-band emissivity over a Virginia pine tree stand before and after removal of a surface litter layer at (a) Plot A and (b) Plot B.

TABLE VI
AVERAGE TP READINGS BEFORE AND AFTER LITTER REMOVAL. LITTER WAS REMOVED FROM PLOT A ONLY

ANGLE OF INCIDENCE [DEGREES]	FOOTPRINT AVERAGE TP READINGS [$cm^3.cm^{-3}$]			
	PLOT A		PLOT B	
	BEFORE	AFTER	BEFORE	AFTER
15°	0.27	0.24	0.19	0.19
25°	0.25	0.23	0.21	0.21
35°	0.27	0.25	0.19	0.18
45°	0.27	0.25	0.23	0.20
55°	0.27	0.27	0.23	0.21

lower angles) in emissivity in Plot A [Fig. 7(a)]. Up to 0.025 decrease in emissivity was observed at an incidence angle of 15°. This decreased to about 0.007 as the angle of incidence increased to 55°. This decrease in the difference between the plot treatments and the increasing incidence angle is due to the increase in the path length that the waves travel within the vegetation, which increases the canopy attenuation and thereby reduces the sensitivity to the underlying forest floor. As the forest floor gets dried, the emissivity of the ground is expected to increase. However, the effect seen at Plot A was opposite to what would be expected from the change in soil conditions alone (about 0.02 $cm^3 \cdot cm^{-3}$ drier surface after litter removal). It is clear that when the surface litter layer is wet, there is an increase in the overall radiance [16], [17]. This effect is evident for both horizontal and vertical polarizations.

When evaluating the measured microwave observations before and after litter removal, it is also necessary to consider the effect of the removal of the litter layer on the gravimetric calibration provided in (1), which is utilized to separate the VMC's of the single layers. To investigate this effect on the interpretation of TP readings after litter removal, the following procedure was conducted. In a manner similar to the procedure explained in Section II-C, the TP measurements were made at 20 different locations where the litter was removed from the surface. Coincident with the TP measurements, the GMC of the

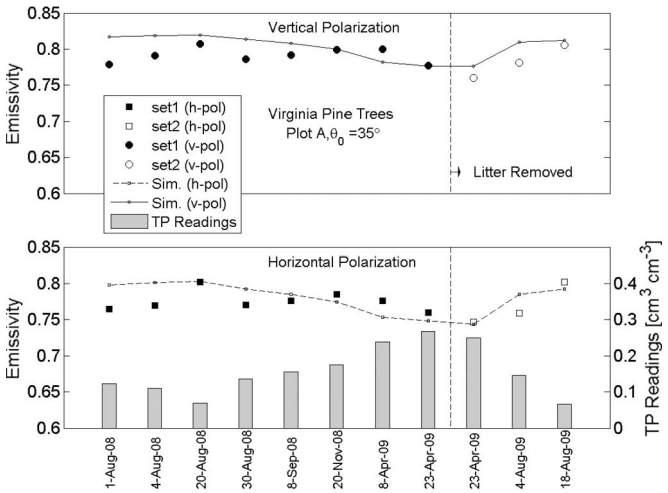

Fig. 8. Simulations are compared with entire microwave data along with ground TP measurements of Plot A. The last three measurements were made after the surface litter was removed on April 23.

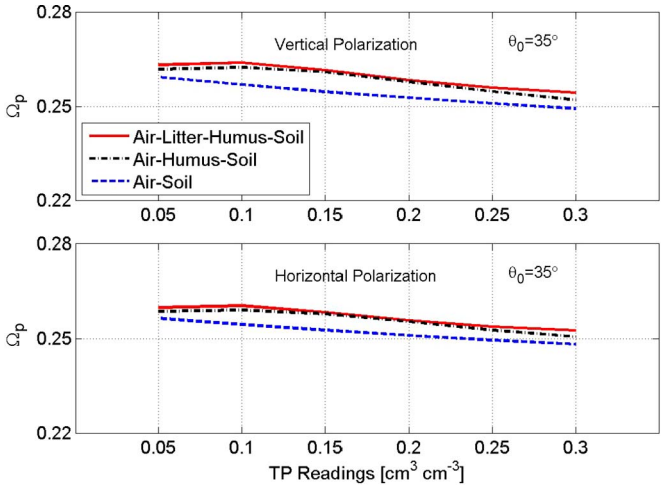

Fig. 9. Effect of forest floor moisture content on the first-order scattering contributions for air–litter–humus–soil, air–humus–soil, and air–soil formations.

humus layer were also measured. Then, the measured GMC values were used in (1b), and TP readings were estimated if they were measured in the presence of litter layer. The estimated TP readings were compared with the measured TP readings in the absence of the litter, and it was found that the comparison of TP readings before and after litter removal (Plot A) was valid within 0.01 $\text{cm}^3 \cdot \text{cm}^{-3}$.

For the summer data acquisitions (on August 1 and 18 in 2009), following the litter removal experiment, standard microwave data along with ground truth were also obtained for both plots. A good dynamic range of ground moisture content was encountered for these days, which was similar to the range of measurements encountered during the campaign before the litter removal experiment. Fig. 8 is a temporal plot of average emissivities along with average TP readings for the entire duration of the campaign in Plot A at an incidence angle of 35°. In the figure, the litter removal experiment day is marked with a vertical dashed line. Data set 1 (the filled markers) was collected before the litter removal, and data set 2 (the non-filled markers) was collected after the litter removal. Average measured TP readings (gray vertical bars) are also provided to indicate the forest floor conditions on each day. The solid curve is the simulated first-order emissivity at vertical polarization while the dashed curve is the simulated horizontally polarized first-order emissivity. The same vegetation parameters given in Table V are used in the simulations for all measurement days. The values of vegetation optical depth for horizontal and vertical polarizations were calculated to be 1.09 and 1.07, respectively, and the single scattering albedo values for horizontal and vertical polarizations were calculated to be 0.62 and 0.61, respectively, at an incidence angle of 35°. Both quantities depend weakly on the angle of incidence and polarization due to the horizontal orientation of primary branches, which are the main source of scattering and extinction [37].

As seen in Fig. 8, the first-order RT model produces a good agreement with the experimental data over the entire experiment duration with limited discrepancies such as the trend from August 30 to November 20. The model predicts that emissivity decreases (increases) with increasing (decreasing) VMC. The increase in measured emissivity on September 8 and November 20 conflicts with the model predictions because there is a decrease in the emissivity as the forest floor gets wetter. The model predictions are expected to be valid under the condition that tree state does not change but moisture content is increased. However, there is supporting evidence that the tree state might be different for these days as opposed to the rest of the measurement days; however, this is not possible to quantify with the available information. For example, the remnants of tropical storm Hannah came through the site a day before the experiment in September and brought 50 mm of rainfall in one day with strong winds up to 80 km/h in the region. The experiment on November 20 represents different seasonal characteristics, and the scene temperature was near freezing. In Fig. 8, it was also observed that the model captures the decrease in horizontal polarized emissivity associated with the removal of the surface litter layer on April 23. The modeled response to combination of both litter removal and slight decrease in ground moisture is lower than the experimental observation for horizontal polarization and somewhat flat for vertical polarization.

The first-order scattering is significant for tree canopies, and it balances the reduction due to the large scattering albedo which is around 0.6. Fig. 9 shows plots of the first-order scattering contributions [see (2b)] for air–litter–humus–soil, air–humus–soil, and air–soil formations separately over a typical range of *TP* readings of 0.05–0.30 $\text{cm}^3 \cdot \text{cm}^{-3}$ at an observation angle of 35°. The purpose of this figure is to provide some insights into the relative importance of organic layers on the first-order scattering contribution. As seen in the plots, the addition of organic layers on top of the mineral soils produces an increase in the scattering term for both polarizations, but the increase due to addition of litter on top of the humus layer is limited. The plots also indicate that the scattering term demonstrates a slightly decreasing trend with TP readings. There are two competing factors for this result: 1) The terms involving ground reflections (sr1) increase with wetter ground, but they are generally negligible compared with direct

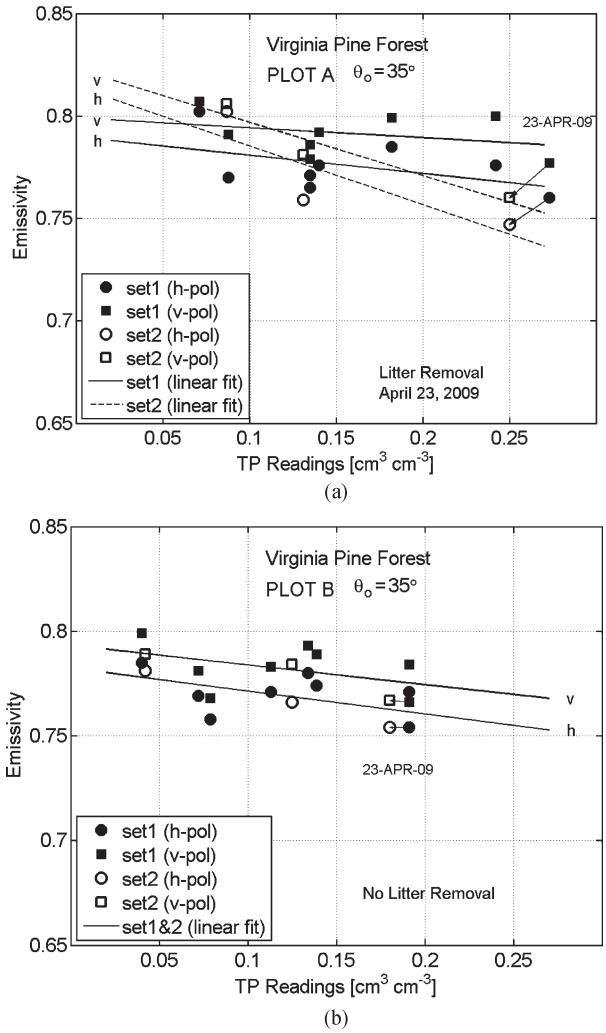

Fig. 10. Microwave observations at angle of 35° from (a) Plot A and (b) Plot B during the entire field campaign.

scattered terms (s1), and 2) the direct scattered ground emission (G-s1) decreases slowly with increasing ground moisture and it is one of the dominating terms contributing to the first-order scattering [19]. As a result, the overall first-order contribution exhibits a fairly constant (slight decreasing) trend over a wide range of ground moisture conditions that could lead to the parameterization of the first-order scattering term with respect to the presence of a litter layer irrespective of any knowledge of the moisture content of the underlying soil.

In Fig. 10, the measured emissivity over the trees for both plots is shown as a function of TP readings for the entire duration of the campaign. The figure shows only the results at an incidence angle of 35°—similar results were also obtained at other incidence angles but are not shown here. The radiometric data collected on April 23 is marked with an arrow. The solid lines represent linear fits to the data collected with a litter layer while dashed lines represent linear fits to the data collected without litter layer. The figure shows that there is limited radiometric sensitivity to changes in soil or litter moisture through the canopy of the pine trees. The radiometer ground moisture sensitivity (change in emissivity per change in TP readings) for both polarizations is 0.20 $[\text{cm}^3 \cdot \text{cm}^{-3}]^{-1}$ in Plot B for the entire duration and in Plot A before litter removal. The sensitivity increases to 0.31 $[\text{cm}^3 \cdot \text{cm}^{-3}]^{-1}$ in Plot A after litter removal. This figure also indicates that the effect of surface litter is more evident when the litter is wet while the effect is negligible under dry conditions.

V. Summary and Conclusion

This paper has presented both theoretical and experimental data concerning the problem of litter effects on the L-band microwave radiometry of forest canopies. A field campaign was described in which L-band passive microwave observations were obtained over a natural Virginia Pine forest, together with ground measurements of the tree biophysical parameters and forest floor characteristics. Microwave measurements were acquired from above the canopy at several look angles by a ground-based microwave instrument system in 2008/2009. Microwave data collection was made on ten different days over a year to include temporal information on ground properties. The radiometric sensitivity to the underlying ground moisture through the pine tree canopy was somewhat limited even though the *VMC* of the ground varied from 0.05–0.30 $\text{cm}^3 \cdot \text{cm}^{-3}$. On a day with wet soil conditions, an experiment was conducted in which the surface litter layer was removed from one half of the test site within a short period of time while keeping the other half undisturbed. Considerable change in brightness temperature was observed after the litter was removed.

The forest floor is made up of organic matter generated by the canopy. This material was characterized by loose debris/needles litter layer, and partially and fully decomposed transition humus layer, lying immediately above the mineral soil. A three-phase dielectric mixing model was adapted to the problem of estimating the effective dielectric properties of the surface litter layer. A new representation of the multilayer forest floor model was incorporated into a recently developed first-order emission model for conifer trees. The model predictions were in good agreement with the data, with limited discrepancies, and provided a quantitative understanding of the influence of organic layers on the first-order brightness temperature. Observations and model results showed that addition of organic layers on top of the mineral soils produces an increase in the overall emission and the first-order scattering contribution. The lack of ground moisture sensitivity was attributed to the presence of the vegetation and surface litter layer which masks soil emission. The effect of surface litter is found to be more evident when the litter is wet and negligible under dry conditions. It is clear that the presence of a litter layer will adversely affect SM estimation unless adequately accounted for in the SM retrieval process.

Appendix
Three-Phase Dielectric Mixing Model of Surface Needle Litter

This Appendix adapts a three-phase dielectric mixing model [33] to the problem of estimating the effective dielectric properties of the surface litter layer. It is assumed that the mixture consists of inclusions made up of water-coated needlelike confocal ellipsoids which are embedded in air and situated in

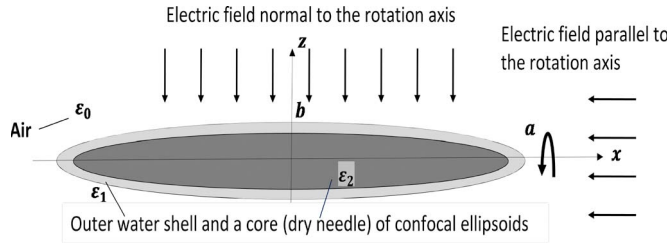

Fig. 11. Effective permittivity of the anisotropic three-phase confocal system of ellipsoids.

all directions parallel to the soil–surface plane, as shown in Fig. 2(b). The ellipsoids have core axial dimension a_2 with two common axial dimensions b_2 and c_2 (i.e., $b_2 = c_2 \ll a_2$) as shown in Fig. 11. The outer ellipsoid is described in Cartesian coordinates by a cubic equation in u (scalar) as

$$\frac{x^2}{u+a_2^2} + \frac{y^2}{u+b_2^2} + \frac{z^2}{u+c_2^2} = 1 \tag{A1}$$

where x, y, and x are the position coordinates of any point on the surface of the ellipsoid and the thickness of the confocal shell is described by adjusting u. The volume of the outer ellipsoid is $V_1 = (4\pi/3)\sqrt{(u+a_2^2)(u+b_2^2)(u+c_2^2)}$ while the volume of the core ellipsoid is $V_2 = (4\pi/3)a_2b_2c_2$. Note that confocal ellipsoids do not have the same axis ratios. Instead, the outer ellipsoid is "fatter" than the inner one.

The application of a mixing scheme based on Maxwell Garnet theory [38] leads to the effective permittivity in horizontal direction ($x-y$ plane)

$$\varepsilon_{Lx}^{\text{eff}} = \varepsilon_{Ly}^{\text{eff}} = \varepsilon_0 + \frac{\varepsilon_0}{2}\frac{\sum_{j=a,b}\frac{n\alpha^j}{\varepsilon_0}}{1-\frac{1}{2}\sum_{j=a,b}N_1^j\frac{n\alpha^j}{\varepsilon_0}} \tag{A2a}$$

and the effective permittivity in vertical direction (z-axis)

$$\varepsilon_{Lz}^{\text{eff}} = \varepsilon_0 + \varepsilon_0\frac{\frac{n\alpha^b}{\varepsilon_0}}{1-N_1^b\frac{n\alpha^b}{\varepsilon_0}} \tag{A2b}$$

where n is the number density, α^j is the polarizability of the anisotropic three-phase confocal system of ellipsoids in j direction, and N_1^j is the depolarization factor of the outer ellipsoids in j direction [39], [40]. An analytical expression for the polarizability factor of layered confocal ellipsoids was derived in [33] and given by

$$\frac{n\alpha^j}{\varepsilon_0} = f_1\frac{(\varepsilon_1-\varepsilon_0)+\left[\varepsilon_1+N_1^j(\varepsilon_0-\varepsilon_1)\right]\frac{(\varepsilon_2-\varepsilon_1)f_2}{\varepsilon_1+N_2^j(\varepsilon_2-\varepsilon_1)}}{\varepsilon_0+N_1^j(\varepsilon_1-\varepsilon_0)+N_1^j\left(1-N_1^j\right)(\varepsilon_1-\varepsilon_0)\frac{(\varepsilon_2-\varepsilon_1)f_2}{\varepsilon_1+N_2^j(\varepsilon_2-\varepsilon_1)}} \tag{A3}$$

where N_2^j is the depolarization factor of the inner ellipsoid and f_1 and f_2 are the volume fractions of the inner to outer ellipsoids and inclusion given by $f_2 = V_2/V_1$ and $f_1 = V_1/V_0$, respectively. The volume of the core is V_2, the total volume of the mixture is given by $V_0 = V_2/(1-p)$, and the total volume of the inclusion (the core and shell) is $V_1 = VMC \times V_0 + V_2$, where porosity is given by $p = 1 - \rho_b/\rho_s$ with bulk density ρ_b and particle density ρ_s. The site-specific bulk densities are given in Section II-C, and the particle densities of organic matter of pine forest and of mineral materials are taken to be 1.43 and 2.65 g $\cdot$ cm^{-3}, respectively [24]. As seen in (A3), the polarizability factor is a function of dielectric constants of inclusions ($\varepsilon_0 = 1$ for air, $\varepsilon_1 = \varepsilon_{bW}$ for water, and $\varepsilon_2 = 2$ for dry needle), depolarization factors of inner and outer ellipsoids, and volume fractions of the inner to outer ellipsoids and inclusion.

In organic soils, bulk density, and thus, also porosity, substantially affects the relationship between the dielectric constant and moisture content. When water molecules make up vicinal layers near solid surfaces, their mobility is reduced by the interaction with solid molecules compared with water in "free" state. The bound water shell is characterized by a reduced permittivity ε_{bW} [28]. In order to account for the reduced permittivity of bound water in the mixing scheme, a water-shell-thickness-dependent approach is adapted here [41]. In this approach, an exponential approximation is used for describing the water phase permittivity starting from a minimum ($\varepsilon_{\min} = 5$) near the surfaces toward the free water phase (ε_{fW}) permittivity at the air interface, resulting in

$$\varepsilon_{bW} = \frac{u\varepsilon_{fW}}{u + \frac{1}{\lambda}\ln\left[\frac{\varepsilon_{fW}-(\varepsilon_{fW}-\varepsilon_{\min})e^{-\lambda u}}{\varepsilon_{\min}}\right]} \tag{A4}$$

where λ is an empirical decay factor taken to be 10^8 m^{-1} and the permittivity ε_{fW} of "free" water is calculated by using a temperature- and salinity-dependent empirical model [42].

REFERENCES

[1] Y. H. Kerr, P. Waldteufel, J. P. Wigneron, S. Delwart, F. Cabot, J. Boutin, M. J. Escorihuela, J. Font, N. Reul, C. Gruhier, S. E. Juglea, M. R. Drinkwater, A. Hahne, M. Martin-Neira, and S. Mecklenburg, "The SMOS mission: New tool for monitoring key elements of the global water cycle," *Proc. IEEE*, vol. 98, no. 5, pp. 666–687, May 2010.

[2] D. Entekhabi, E. Njoku, P. E. O'Neill, K. Kellogg, W. Crow, W. Edelstein, J. Entin, S. Goodman, T. Jackson, J. Johnson, J. Kimball, J. Piepmeier, R. Koster, N. Martin, K. McDonald, M. Moghaddam, S. Moran, R. Reichle, J. C. Shi, M. Spencer, S. Thurman, L. Tsang, and V. Jakob, "The Soil Moisture Active and Passive (SMAP) mission," *Proc. IEEE*, vol. 98, no. 5, pp. 704–716, May 2010.

[3] R. H. Lang, C. Utku, P. de Matthaeis, N. Chauhan, and D. M. LeVine, "ESTAR and model brightness temperatures over forests: Effects of soil moisture," in *Proc. IEEE IGARSS*, Jul. 2001, vol. 3, pp. 1300–1302.

[4] G. Macelloni, S. Paloscia, P. Pampaloni, and R. Ruisi, "Airborne multifrequency L- to Ka-band radiometric measurements over forests," *IEEE Trans. Geosci. Remote Sens.*, vol. 39, no. 11, pp. 2507–2513, Nov. 2001.

[5] J. P. Grant, J. P. Wigneron, A. A. Van de Griend, A. Kruszewski, S. Schmidl Sobjerg, and N. Skou, "A field experiment on microwave forest radiometry: L-band signal behavior for varying conditions of surface wetness," *Remote Sens. Environ.*, vol. 109, no. 1, pp. 10–19, Jul. 2007.

[6] P. E. O'Neill, R. H. Lang, M. Kurum, A. T. Joseph, T. J. Jackson, M. H. Cosh, and R. Nelson, "ComRAD active/passive microwave measurements of tree canopies," in *Proc. IEEE IGARSS*, Barcelona, Spain, Jul. 2007, pp. 1420–1423.

[7] M. Guglielmetti, M. Schwank, C. Mätzler, C. Oberdörster, J. Vanderborght, and H. Fluhler, "Measured microwave radiative transfer properties of a deciduous forest canopy," *Remote Sens. Environ.*, vol. 109, no. 4, pp. 523–532, Aug. 2007.

[8] M. Guglielmetti, M. Schwank, C. Matzler, C. Oberdorster, J. Vanderborght, and H. Fluhler, "FOSMEX: Forest soil moisture experiments with microwave radiometry," *IEEE Trans. Geosci. Remote Sens.*, vol. 46, no. 3, pp. 727–735, Mar. 2008.

[9] J. P. Grant, K. Saleh, J. P. Wigneron, M. Guglielmetti, Y. Kerr, M. Schwank, N. Skou, and A. A. Van de Griend, "Calibration of the L-MEB model over a coniferous and a deciduous forest," *IEEE Trans. Geosci. Remote Sens.*, vol. 46, no. 3, pp. 808–818, Mar. 2008.

[10] J. P. Grant, A. A. Van de Griend, M. Schwank, and J. P. Wigneron, "Observations and modeling of a pine forest floor at L-band," *IEEE Trans. Geosci. Remote Sens.*, vol. 47, no. 7, pp. 2024–2034, Jul. 2009.
[11] E. Santi, S. Paloscia, P. Pampaloni, and S. Pettinato, "Ground-based microwave investigations of forest plots in Italy," *IEEE Trans. Geosci. Remote Sens.*, vol. 47, no. 9, pp. 3016–3025, Sep. 2009.
[12] P. Ferrazzoli and L. Guerriero, "Passive microwave remote sensing of forests: A model investigation," *IEEE Trans. Geosci. Remote Sens.*, vol. 34, no. 2, pp. 433–443, Mar. 1996.
[13] M. A. Karam, "A physical model for microwave radiometry of vegetation," *IEEE Trans. Geosci. Remote Sens.*, vol. 35, no. 4, pp. 1045–1058, Jul. 1997.
[14] P. Ferrazolli, L. Guerriero, and J. P. Wigneron, "Simulating L-band emission of forests in view of future satellite applications," *IEEE Trans. Geosci. Remote Sens.*, vol. 40, no. 12, pp. 2700–2708, Dec. 2002.
[15] R. H. Lang, N. Chauhan, C. Utku, and D. M. Le Vine, "L-band active and passive sensing of soil moisture through forests," in *Proc. IEEE MicroRad*, San Juan, PR, Aug. 2006, pp. 193–196.
[16] A. Della Vecchia, P. Ferrazzoli, J. P. Wigneron, and J. P. Grant, "Modeling forest emissivity at L-band and a comparison with multitemporal measurements," *IEEE Geosci. Remote Sens. Lett.*, vol. 4, no. 4, pp. 508–512, Oct. 2007.
[17] M. Schwank, M. Guglielmetti, C. Matzler, and H. Fluhler, "Testing a new model for the L-band radiation of moist leaf litter," *IEEE Trans. Geosci. Remote Sens.*, vol. 46, no. 7, pp. 1982–1994, Jul. 2008.
[18] A. Della Vecchia, P. Ferrazzoli, L. Guerriero, R. Rahmoune, S. Paloscia, S. Pettinato, and E. Santi, "Modeling the multifrequency emission of broadleaf forests and their components," *IEEE Trans. Geosci. Remote Sens.*, vol. 48, no. 1, pp. 260–272, Jan. 2010.
[19] M. Kurum, R. H. Lang, P. O'Neill, A. Joseph, T. Jackson, and M. Cosh, "A first-order radiative transfer model for microwave radiometry of forest canopies at L-band," *IEEE Trans. Geosci. Remote Sens.*, vol. 49, no. 9, pp. 3167–3179, Sep. 2011.
[20] K. Saleh, J. P. Wigneron, P. de Rosnay, J. C. Calvet, M. J. Escorihuela, Y. Kerr, and P. Waldteufeld, "Impact of rain interception by vegetation and mulch on the L-band emission of natural grass," *Remote Sens. Environ.*, vol. 101, no. 1, pp. 127–139, Mar. 2006.
[21] V. N. Kleshchenko, S. A. Komarov, and V. L. Mironov, "Dielectric properties of needle litter," *J. Commun. Technol. Electron.*, vol. 47, no. 11, pp. 1202–1205, 2002.
[22] F. Demontoux, B. Le Crom, G. Ruffié, J. P. Wigneron, J. P. Grant, V. L. Mironov, and H. Lawrence, "Electromagnetic characterization of soil-litter media: Application to the simulation of the microwave emissivity of the ground surface in forests," *Eur. Phys. J. Appl. Phys.*, vol. 44, no. 3, pp. 303–315, Dec. 2008.
[23] P. E. O'Neill, R. H. Lang, M. Kurum, K. R. Carver, and C. Utku, "Multi-sensor microwave remote sensing of NASA's Combined Radar/Radiometer (ComRAD) system," in *Proc. IEEE MicroRad*, San Juan, PR, Feb. 2006, pp. 50–54.
[24] T. E. Redding, K. D. Hannamb, S. A. Quideaub, and K. J. Devitoa, "Particle density of aspen, spruce, and pine forest floors in Alberta, Canada," *Soil Sci. Soc. Amer. J.*, vol. 69, no. 5, pp. 1503–1506, Aug. 2005.
[25] J. R. Birchak, C. G. Gardner, J. E. Hipp, and J. M. Victor, "High dielectric constant microwave probes for sensing soil moisture," *Proc. IEEE*, vol. 62, no. 1, pp. 93–98, Jan. 1974.
[26] G. C. Topp, J. L. Davis, and A. P. Annan, "Electromagnetic determination of soil water content: Measurements in coaxial transmission lines," *Water Resource Res.*, vol. 16, no. 3, pp. 574–582, 1980.
[27] J. R. Wang and T. J. Schmugge, "An empirical model for the complex dielectric permittivity of soils as a function of water content," *IEEE Trans. Geosci. Remote Sens.*, vol. GRS-18, no. 4, pp. 288–295, Oct. 1980.
[28] M. C. Dobson, F. T. Ulaby, M. T. Hallikainen, and M. A. El-Rayes, "Microwave dielectric behavior of wet soil—Part II: Dielectric mixing models," *IEEE Trans. Geosci. Remote Sens.*, vol. GRS-23, no. 1, pp. 35–46, Jan. 1985.
[29] K. Roth, R. Schulin, H. Flühler, and W. Attinger, "Calibration of time domain reflectometry for water content measurement using a composite dielectric approach," *Water Resources Res.*, vol. 26, no. 10, pp. 2267–2273, 1990.
[30] M. A. Malicki, R. Plagge, and C. H. Roth, "Influence of matrix on TDR soil moisture readings and its elimination," in *Proc. Symp. Workshop Time Domain Reflectometry Environ., Infrastructure, Mining Appl. Evanston, IL, Special Publ. SP19-94 US Dept. Interior*, Washington, DC, Sep. 1994, pp. 294–308, Bureau of Mines.
[31] M. G. Schaap, L. de Lange, and T. J. Heimovaara, "TDR calibration of organic forest floor media," *Soil Technol.*, vol. 11, no. 2, pp. 205–217, Jun. 1997.
[32] D. Canone, M. Previati, S. Ferraris, and R. Haverkamp, "A new coaxial time domain reflectometry probe for water content measurement in forest floor litter," *Vadose Zone J. Soil Sci. Soc. Amer.*, vol. 8, no. 2, pp. 363–372, May 2009.
[33] A. Sihvola and I. V. Lindell, "Polarizability and effective permittivity of layered and continuously inhomogeneous dielectric ellipsoids," *J. Electromagn. Waves Appl.*, vol. 4, no. 1, pp. 1–26, Jan. 1990.
[34] F. T. Ulaby and R. P. Jedlicka, "Microwave dielectric properties of plant materials," *IEEE Trans. Geosci. Remote Sens.*, vol. GRS-22, no. 4, pp. 406–415, Jul. 1984.
[35] M. Born and E. Wolf, *Principles of Optics: Electromagnetic Theory of Propagation, Interference and Diffraction of Light*, 7th ed. Cambridge, U.K.: Cambridge Univ. Press, 1999, ch. 1.
[36] B. J. Choudhury, T. J. Schmugge, R. W. Newton, and A. Chang, "Effect of surface roughness on the microwave emission from soils," *J. Geophys. Res.*, vol. 84, no. C9, pp. 5699–5706, Sep. 1979.
[37] M. Kurum, P. E. O'Neill, R. H. Lang, A. T. Joseph, M. H. Cosh, and T. J. Jackson, "Characterization of forest opacity using multi-angular emission and backscatter data," in *Proc. Int. Geosci. Remote Sens. Symp.*, Honolulu, HI, Jul. 25–30, 2010, pp. 2051–2054.
[38] J. C. Maxwell-Garnett, "Colors in metal glasses and metallic films," *Philos. Trans. R. Soc. London Ser. A*, ser. 203, pp. 385–420, 1904.
[39] E. C. Stoner, "The demagnetizing factors for ellipsoids," *Philosoph. Mag. Ser. 7*, vol. 36, no. 263, pp. 803–821, 1945, 1941-5990.
[40] J. A. Osborn, "Demagnetizing factors of the general ellipsoid," *Phys. Rev.*, vol. 67, no. 11/12, pp. 351–357, Jun. 1945.
[41] S. P. Friedman, "A saturation degree-dependent composite spheres model for describing the effective dielectric constant of unsaturated porous media," *Water Resources Res.*, vol. 34, no. 11, pp. 2949–2961, 1998.
[42] L. A. Klein and C. T. Swift, "An improved model for the dielectric constant of sea water at microwave frequencies," *IEEE Trans. Antennas Propag.*, vol. AP-25, no. 1, pp. 104–111, Jan. 1977.

Mehmet Kurum (S'08–M'09) received the B.S. degree in electrical and electronics engineering from BogaziUniversity, Istanbul, Turkey, in 2003 and the M.S. and Ph.D. degrees in electrical engineering from The George Washington University (GWU), Washington, DC, in 2005 and 2009, respectively.

During his graduate studies, he was a Research Assistant with GWU, where he conducted research in the radar time-domain characterization of wave propagation in forested landscapes, in the development of the National Aeronautics and Space Administration (NASA)'s ComRAD system, in the design of network-analyzer-based radar for NASA's 2-km microwave link, and in the development of algorithms to measure rainfall over the link. Since 2009, he has been with the Hydrological Sciences Branch, Hydrospheric and Biospheric Sciences Laboratory, NASA Goddard Space Flight Center, Greenbelt, MD, where he conducted research in correcting the forest canopy effects on active/passive microwave remote sensing of soil moisture.

Peggy E. O'Neill (M'85–SM'03) received the B.S. degree (*summa cum laude*, with university honors) from Northern Illinois University, DeKalb, in 1976 and the M.A. degree from the University of California, Santa Barbara, in 1979, all in geography.

She also spent a year with Cornell University, Ithaca, NY, where she did postgraduate work in civil and environmental engineering. Since 1980, she has been a Physical Scientist with the Hydrological Sciences Branch, Hydrospheric and Biospheric Sciences Laboratory, National Aeronautics and Space Administration (NASA)/Goddard Space Flight Center, Greenbelt, MD, where she conducted research in soil moisture retrieval and land surface hydrology, primarily through microwave remote sensing techniques. She is currently a Deputy Project Scientist for NASA's SMAP soil moisture mission.

Roger H. Lang (F'89) received the B.S. and M.S. degrees in electrical engineering and the Ph.D. degree in electrophysics from the Polytechnic Institute of New York University, Brooklyn, in 1962, 1964, and 1968, respectively.

From 1963 to 1964, he was with Bell Telephone Laboratories, where he worked on satellite antennas. From 1968 to 1970, he was with the Courant Institute of Mathematical Sciences, New York University, where he did postdoctoral work on wave propagation in random media. He is currently the L. Stanley Crane Professor of engineering and applied science with the George Washington University, Washington, DC. He has worked with the National Aeronautics and Space Administration for many years on microwave remote sensing and is currently on the Aquarius science team.

Dr. Lang is a member of the editorial board of *Waves in Random and Complex Media*. He has been a member of the Ad Com committee of the IEEE Geoscience and Remote Sensing Society and an Associate Editor for IEEE TRANSACTIONS ON GEOSCIENCE AND REMOTE SENSING. He is currently the Vice Chairman of International Union of Radio Science Commission F.

Michael H. Cosh received the B.A. degree in engineering, with minors in math and physics, from Saint Francis College, Loretto, PA, in 1995; the B.S. degree (*magna cum laude*, with honors) in civil and environmental engineering from The Pennsylvania State University, University Park, in 1996; and the M.S. degree in hydraulics and hydrology and the Ph.D. degree in environmental fluid mechanics and hydrology from the School of Civil and Environmental Engineering, Cornell University, Ithaca, NY, in 1998 and 2002, respectively.

He is currently with the Hydrology and Remote Sensing Laboratory, U.S. Department of Agriculture Agricultural Research Service, Beltsville, MD. His research interest include *in situ* soil moisture network validation, scaling of land surface parameters to satellite scale, and leaf wetness characterization and its interaction with microwave remote sensing.

Alicia T. Joseph received the B.S. degree in environmental science from Medgar Evers College, City University of New York, Brooklyn, in 1998; the M.S. degree in environmental and occupational health science from Hunter College, City University of New York, New York, in 2000; the M.S. degree in geography and environmental engineering from The Johns Hopkins University, Baltimore, MD, in 2004; and the Ph.D. degree with a research topic in "Physical and Semi-Empirical Approaches to Quantifying Microwave Optical Depth of Vegetation to Improve Estimates of Soil Moisture" in the University of Maryland, College Park.

Since 2001, she has been with the Hydrological Sciences Branch, Hydrospheric and Biospheric Sciences Laboratory, National Aeronautics and Space Administration Goddard Space Flight Center, Greenbelt, MD, where she conducted research in the microwave remote sensing of soil moisture retrieval.

Thomas J. Jackson (A'86–M'96–F'02) received the Ph.D. degree from the University of Maryland, College Park, in 1976.

Since 1977, he has been with the Agricultural Research Service (ARS), Beltsville, MD. He is or has been a member of the science and validation teams of the Aqua, ADEOS-II, Radarsat, Oceansat-1, Envisat, ALOS, and SMOS remote sensing satellites. He is currently a Research Hydrologist with the Hydrology and Remote Sensing Laboratory, U.S. Department of Agriculture, ARS. His research interests include the application and development of remote sensing technology in hydrology and agriculture, primarily microwave measurement of soil moisture.

Dr. Jackson is a Fellow of the American Meteorological Society and the American Geophysical Union. He was the recipient of the AGU Hydrology Award and the William T. Pecora Award (NASA and Department of Interior) for his outstanding contributions toward understanding the Earth by means of remote sensing in 2003. He is a member of the IEEE Geoscience and Remote Sensing Administrative Committee, where he serves as a Secretary.